Quantifying the consistency and rheology of liquid foods using fractional calculus

Caroline E. Wagner [*1], Alexander C. Barbati [†1], Jan Engmann [‡2], Adam S. Burbidge [§2], and Gareth H. McKinley [¶1]

[1]Hatsopoulos Microfluids Laboratory, Department of Mechanical Engineering, Massachusetts Institute of Technology, Cambridge, MA 02139, USA

[2]Nestlé Research Center, Vers-chez-les-Blanc PO Box 44, 1000 Lausanne 26, Switzerland

January 23, 2017

Abstract

It is well known that the perceived texture and consistency of liquid foods are strong drivers of consumer preference, yet quantification of these parameters is made complicated by the absence of a concise mathematical framework. In this paper, we demonstrate that fractional rheological models, including the fractional Maxwell model (FMM) and the fractional Jeffreys model (FJM), are potential candidates to fill this void as a result of their ability to succinctly and accurately predict the linear and nonlinear viscoelastic response of a range of liquid food solutions. These include a benchmark fluid, the dysphagia product Resource ® Thicken Up Clear, various plant extracts whose constituent polysaccharides have been reported to impart significant viscoelasticity, and human whole saliva. These fractional constitutive models quantitatively describe both the linear viscoelasticity of all of the liquid foods as well as the shear thinning of their steady shear viscosity (through application of the Cox-Merz rule), and outperform conventional multi-mode Maxwell models with up to 50 physical elements in terms of the goodness of fit to experimental data. Further, by accurately capturing the shear viscosity of the various liquid food solutions at the shear rate of $\dot{\gamma} = 50\,\mathrm{s}^{-1}$ (widely deemed relevant for oral

[*]cewagner@mit.edu
[†]barbati@mit.edu
[‡]jan.engmann@rdls.nestle.com
[§]adam.burbidge@rdls.nestle.com
[¶]gareth@mit.edu

evaluation of liquid texture), we show that two of the constitutive parameters of the fractional Maxwell model can be used to construct a state diagram that succinctly characterizes both the viscous and elastic properties of the different fluids. This characterization facilitates the assignment of quantitative values to largely heuristic food textural terms, which may improve the design of future liquid foods of specific desired consistencies or properties.

1 Introduction

For many food products, textural attributes are strong drivers of consumer preference [1]. In addition to the importance for the sensory experience associated with food, texture plays a critical role in determining what can and cannot be consumed for people suffering from mastication and swallowing disorders, which are collectively known as dysphagia [2, 3, 4]. As a result of the difficulty that many of these patients have with swallowing very tough foods such as meat, softer diets are commonly followed [4]. Moreover, higher viscosity, 'thicker', liquids are generally preferred over 'thinner' ones due to the increased risk of aspirating thin liquids [2].

Quantification of food consistency is complicated by at least two important factors, however: i) the inevitable variations in perceived texture across individuals, and ii) the absence of a concise mathematical framework and robust set of measurable parameters for doing so. As an illustrative example of individual variations, at a lecture delivered in 1970 at the Technical University in Budapest, the English rheologist G. W. Scott Blair noted that since the French 'seldom spread jam on their bread', texture and hole density play a diminished role compared to taste in their enjoyment of bread, resulting in consistency being a much larger concern for bread-makers selling their fare to jam-spreading Britons [5].

To assess concepts such as consistency, sensory panel testing requires a number of individuals to consume a product in a well-controlled manner and rate various 'sensory attributes' against a given standard. For example, one could attempt to quantify the crunchiness of an apple on a numerical scale for which a ripe peach is a 1 and a really fresh stick of celery is a 10. Each individual will likely show differences in sensory perception, rendering such attributes difficult (if not impossible) to measure objectively. An additional consideration relates to common reference points. Unlike for simple colours and sound, for example, such references are not obvious for oral mechanoreception, where the medium to be sensed needs to be moved and manipulated inside the oral cavity to reach the locations where it is sensed (tongue, palate, cheeks,

etc...). This manipulation in the oral cavity is likely to vary from person to person, and is consequently difficult to standardize.

To address the second issue, the development of a mathematical framework for the quantification of food consistency to reduce the need for subjective assessments is needed. Food materials are generally inhomogeneous and exhibit markedly different properties depending on the time- and length-scales of observation. This structural complexity adds some difficulties for material characterization; in general, simple physical laws such as Newton's law of viscosity for liquids and Hooke's law for elastic solids are insufficient [6, 7]. A classical approach to develop models for rheologically complex materials has been to conceptualise networks of springs and dashpots to incorporate elements capturing both an elastic and a viscous response in the sample stress as it responds to imposed deformations [8]. Classic examples include the Maxwell model (one spring and one dashpot in series), which has been successfully applied to polymer fluids for small displacement gradients, as well as the Kelvin-Voigt model (one spring and one dashpot in parallel), which can compactly describe the creep of solid-like materials [8].

These constitutive formulations have also been employed in the characterization of food rheology, for instance, Schofield and Scott Blair used an intricate network of springs to model the response of gluten and starch in bread dough [9]. Kokini [10] investigated the applicability of a range of constitutive equations in rheological studies of pectin solutions and gluten doughs. While he was able to adequately model the rheological response of the individual foods using specifically tailored models, he concluded that 'new models need to be designed which are capable of accounting for the diverse and complex structural properties of foods'.

To this end, fractional rheological models, originally pioneered by Nutting and Scott Blair [6, 11, 12], have proven to be a concise and elegant framework for predicting the response of complex fluids such as liquid foods using a small number of parameters. The introduction of what Scott Blair called *quasiproperties* [6], i.e. material parameters that interpolate between a viscosity and an elastic modulus, as well as the incorporation of fractional time derivatives of the imposed strain and resulting stress, offers a compact alternative to fitting a spectrum of material constants to the numerous length and time scales typically found in many complex fluids [7].

Originally, Scott Blair and coworkers applied these models towards the classification of industrial materials such as rubber and bitumen [13, 14]. Since then, their utility in the field of food rheology has also been recognized[1]. Oroian et al. have modeled the linear viscoelastic response of honey using a fractional rheological model [15], while Song et al. applied a similar approach to the modeling of xanthan gum solutions [16]. These latter authors concluded that the weak dependence of the storage and loss moduli on frequency during small amplitude oscillatory shear flows, as measured by the fractional value of the time derivative of the material strain, was an indication of a weak gel-like structure in these xanthan gum solutions. In their studies of product aging, Quinchia et al. have also modeled the linear viscoelastic response of a commercial strawberry pudding using power laws, although the direct connection to fractional calculus was not made at the time by these authors [17]. As a final example, Faber et al. have recently applied fractional models towards the evaluation of the effect of fat and water content on technological measures such as the firmness, rubberiness, and springiness of cheese at different temperatures [18, 19].

In this manuscript, we first use fractional constitutive models to predict the linear and nonlinear viscoelastic response of a well defined, benchmark system designed to produce fluids with specific food textures at appropriate concentrations: the xanthan gum based food-thickening dysphagia product Resource ® Thicken Up Clear (referred to henceforth as TUC) produced by Nestlé. Based on early sensory panel reports of the perceived texture of various starch-based food solutions [20], the National Dysphagia Diet Task Force (NDDTF) classifies food solutions with shear viscosities of $1 \leq \eta \leq 50\,\mathrm{mPa\,s}$ as having a 'thin' consistency, viscosities in the range $51 \leq \eta \leq 350\,\mathrm{mPa\,s}$ are described as having a 'nectar-like' consistency, higher viscosities $351 \leq \eta \leq 1750\,\mathrm{mPa\,s}$ correspond to a 'honey-like' consistency, and $\eta > 1750\,\mathrm{mPa\,s}$ is termed a 'spoon-thick' consistency (also referred to as 'pudding-like'), with all measurements performed at a shear rate of $\dot{\gamma} = 50\,\mathrm{s}^{-1}$ and at 25 °C [2]. We note that in other countries such as the United Kingdom and Australia, the viscosities along which these textural divisions are drawn are similar, but the specific descriptive term associated with each consistency varies [21].

In this paper, we show that the values of the quasiproperties and power law indices of the fractional models describing different concentrations of TUC can be used to quantify the different levels of viscoelasticity associated with each of these descriptors. We then apply this framework towards the characterization of selected plant extracts whose constituent biopolymers are known to impart significant viscoelasticity and show that the rheological response of these materials can also be well described by fractional models.

Examples include extracts from okra plants, chia seeds, and flax seeds, as well as gums typically used in food manufacturing and stabilization, including guar and tara gums [22, 23]. Since we have observed similar trends in the rheological behaviour of whole human saliva (which plays a significant role in mouth-feel and food textural perception [24]), we include a similar analysis of saliva as well. We conclude that in general, the specification of a single shear viscosity at $\dot{\gamma} = 50\,\mathrm{s}^{-1}$ might be insufficient to uniquely capture the rheological response associated with conventional food textural terms such as 'nectar' and 'pudding'. Instead, we show that by quantifying the rheological response of these liquid foodstuffs in terms of two constitutive parameters obtained from the fractional models, a 'consistency phase space' can be developed which allows for an improved mapping of these descriptive textural terms to quantitative values of the material viscoelasticity.

2 Background

2.1 Experimental details

Commercial formulations of Thicken Up Clear (TUC) were purchased from the storefront Treasure Zone on Amazon. Solutions were prepared by combining the appropriate amount of TUC powder with deionized water and then vigorously stirring using a magnetic stir bar at 300 rpm for 3 minutes at room temperature. The solutions were then mixed gently on a roller mixer for 2 hours to insure complete hydration. The procedural details for each of the other biopolymer solutions and saliva are provided in Section 4.

Shear measurements were performed using a TA Instruments (New Castle, DE, USA) stress controlled AR-G2 rheometer with a 60 mm, 2° cone-and-plate fixture. All experiments were performed on a Peltier plate at a constant temperature T = 25 °C. We follow the recent recommendation of Wagner et al. [25] by requiring the accumulation of material strains in excess of $\gamma \geq 5$ in all of the biopolymer solutions before reporting viscosity data during steady state flow measurements. This recommendation was made in response to various reports in the literature of a curious region of shear thickening at low shear rates ($\dot{\gamma} \lesssim 0.1\,\mathrm{s}^{-1}$) in high molecular weight synthetic and biopolymer solutions, leading to an apparent local maximum in the shear viscosity [25]. Wagner et al. demonstrate that when total strains of $\gamma \geq 5$ are allowed to accumulate during each steady state flow measurement at each share rate, proper sample equilibration eliminates this non-monotonic response in the apparent steady shear viscosity [25].

2.2 Theoretical and modeling details

Biological polysaccharides (e.g. guar and tara gum, okra, etc...) possess a polydisperse distribution of polymer chain lengths and a variety of binding/crosslinking and/or macromolecular association mechanisms, producing a microstructure with a seemingly continuous distribution of chain lengths between associative junctions. These features contrast with the classical Green–Tobolsky network model in which a single relaxation mode corresponding to an active elastic segment of a given length (represented mechanically by a spring and dashpot in series) describes the linear viscoelastic response of the physical network. A large ensemble of these Maxwell modes in parallel is required to approximate the experimental response of multi-scale materials like biopolymers, which has been argued by some, including Tschoegl, to lead to a 'loss of physicality' [26].

Balancing the desire for parsimonious and physically meaningful models with accurate descriptions of measured material properties persists as a major challenge in food process engineering, particularly for multi-component and multi-scale materials where an *a priori* understanding or description of the material microstructure is absent. Freund and Ewoldt have recently proposed a fitting regimen using Bayesian statistics to select an optimal rheological model from a pool of pre-defined candidate models [27]. The selection of a single candidate model is driven by the product of two fitness terms: one that reflects the ability of the model to faithfully reproduce the data, and a data independent term reflecting *a priori* knowledge of the model based on physical intuition [27]. These authors argue that fractional models are generally able to reproduce data very well (thus resulting in a high score for the reproducibility term), but claim that physical intuition for fractional models is generally lacking (resulting in a low score for the intuition component) [27]. Despite the subjectiveness of the latter criterion, their Bayesian analysis concludes that for some complex fluids such as gluten gels, models such as the CGRM (Critical Gelation Rouse Model) which can be represented in a compact fractional framework are in fact the most appropriate choice [27]. Further, Bagley has shown in several papers that a broad range of generalized Rouse-Zimm like models can also be represented in the form of fractional viscoelastic constitutive equations [28, 29, 30].

Jaishankar and McKinley [7] have recently demonstrated that the fractional Maxwell model (FMM, depicted schematically in Figure 1a) is very well suited to capture the linear response of aqueous biopolymer solutions such as xanthan gum and the food biopolymer solutions considered in this manuscript. The mathematical details of the FMM are discussed at length elsewhere [7, 31]. Briefly, this model consists

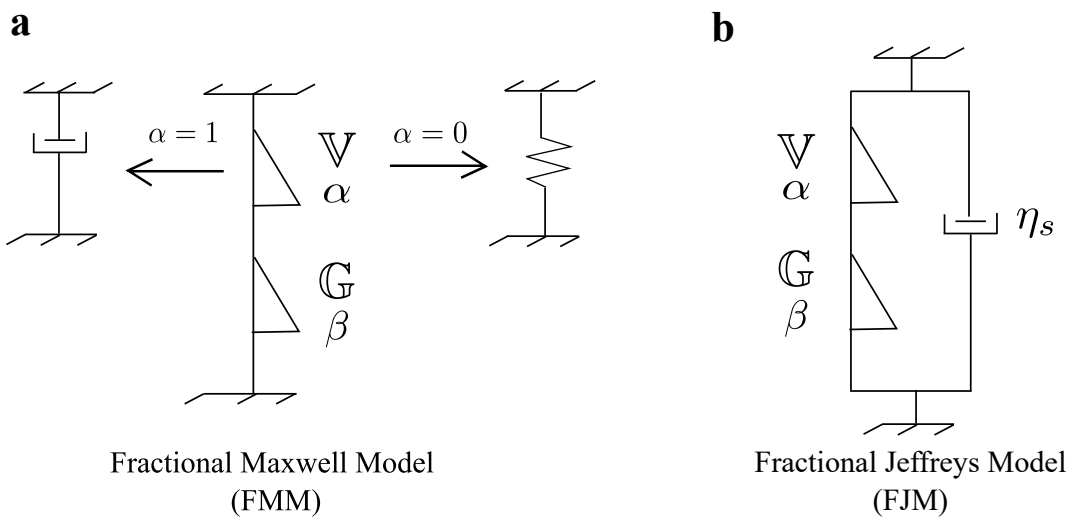

Figure 1: Schematic representation of the fractional Maxwell model (FMM) as two 'springpots' in series and the definition of a springpot as a mechanical element that interpolates between a spring ($\alpha = 0$) and a dashpot ($\alpha = 1$). (b) Fractional Jeffreys model (FJM) with two springpots in series arranged in parallel with a purely viscous (dashpot) element to account for solvent viscosity.

of two springpots (or 'Scott Blair elements') in series. These fractional mechanical elements interpolate between a spring and a dashpot. The first we denote with a quasiproperty $\mathbb{V}$ with units of [Pa s$^\alpha$] and fractional derivative order α, and the second with quasiproperty $\mathbb{G}$ [Pa s$^\beta$] and fractional derivative order β, where we take $0 \leq \beta < \alpha \leq 1$ without loss of generality [7]. We note that while the physical meaning of a quasiproperty is perhaps initially less straightforward to grasp as compared to an elastic modulus or a viscosity, the quasiproperty magnitudes can nevertheless be taken as indicators of the 'stiffness' of the complex fluid in question and the scale of the stress expected in a system once a characteristic timescale or deformation rate is specified. Clearly, when $\alpha \to 1$ and $\beta \to 0$, the classical Maxwell model is recovered (see Figure 1a). In general, the FMM model gives rise to power law responses in the linear viscoelastic relaxation modulus $G(t)$, with the exponent α capturing the slope $\mathrm{d}G(t)/\mathrm{d}t$ at long times (or low frequencies), and the exponent β capturing the slope at short times (or high frequencies) [7]. The FMM expression for the complex modulus $G^*(\omega)$ as a function of frequency is given in compact form [7] as

$$G^*_{FMM}(\omega) = \frac{\mathbb{V}(i\omega)^\alpha \mathbb{G}(i\omega)^\beta}{\mathbb{G}(i\omega)^\alpha + \mathbb{V}(i\omega)^\beta}. \tag{1}$$

The individual components of storage and loss moduli can consequently be obtained by separating the complex modulus into its real and imaginary parts, $G^*(\omega) = G'(\omega) + iG''(\omega)$, yielding

$$G'_{FMM}(\omega) = G'_{FJM}(\omega) = \mathbb{V}\tau^{-\alpha}\frac{(\omega\tau)^{\alpha}\cos(\pi\alpha/2) + (\omega\tau)^{2\alpha-\beta}\cos(\pi\beta/2)}{(\omega\tau)^{2(\alpha-\beta)} + 2(\omega\tau)^{\alpha-\beta}\cos(\pi(\alpha-\beta)/2) + 1} \tag{2}$$

and

$$G''_{FMM}(\omega) = \mathbb{V}\tau^{-\alpha}\frac{(\omega\tau)^{\alpha}\sin(\pi\alpha/2) + (\omega\tau)^{2\alpha-\beta}\sin(\pi\beta/2)}{(\omega\tau)^{2(\alpha-\beta)} + 2(\omega\tau)^{\alpha-\beta}\cos(\pi(\alpha-\beta)/2) + 1}, \tag{3}$$

where $\tau = (\mathbb{V}/\mathbb{G})^{1/(\alpha-\beta)}$ is a characteristic time scale of the FMM [32]. Provided $1 \geq \alpha > 1/2 > \beta \geq 0$, so that the model response is not purely viscous or purely elastic at any point over the entire frequency range, it can be shown that the viscoelastic moduli show a crossover from a dominantly viscous to a dominantly elastic response as the frequency increases [32]. The crossover frequency ω_c at which $G'(\omega_c) = G''(\omega_c)$ can be found by equating Equations (2) and (3), giving an alternate way of determining a single characteristic time of the FMM. The crossover time scale $\tau_c \equiv 1/\omega_c$ is given by the expression [32]:

$$\tau_c = \frac{1}{\omega_c} = \tau\left[\frac{\cos(\pi\beta/2) - \sin(\pi\beta/2)}{\sin(\pi\alpha/2) - \cos(\pi\alpha/2)}\right]^{1/(\alpha-\beta)}. \tag{4}$$

Either τ or τ_c can be used to compactly provide a single scalar metric combining all four constitutive parameters in the FMM. Because τ_c can be related to a visually distinct measure (the crossover frequency at which $G'(\omega_c) = G''(\omega_c)$), we choose to report values in Table 1 using this parameter.

To demonstrate qualitatively and quantitatively the descriptive ability of the FMM over a generalized Maxwell model corresponding to an ensemble of M discrete Maxwell modes (or N = 2M parameters), we compare the cost function of the FMM versus an M-mode Maxwell model describing the linear viscoelastic properties of the $c = 1.2\,\mathrm{wt}\,\%$ preparation of TUC. We undertake this exercise to determine what number, if any, of linear Maxwell modes will model the linear viscoelastic data as well as the 4 parameter FMM. Since the optimal parameter values for each mode of the M-mode Maxwell model are unknown, and the parameter space is increasingly difficult to explore as the number of parameters is increased, we perform repeated minimizations of the cost function

$$\epsilon = \sum_{i=1}^{n_{\mathrm{data}}}\left(\frac{(G'_i - G'_{i,\mathrm{fit}})}{G'_i}\right)^2 + \left(\frac{(G''_i - G''_{i,\mathrm{fit}})}{G''_i}\right)^2 \tag{5}$$

using the genetic algorithm command *ga* in Matlab. For each minimization, we initialize the genetic algorithm with the larger of 300 or 100×M children (where M is the number of Maxwell modes), which

then evolve to determine the best fit to the candidate data. We constrain all initial and evolved model parameters to be positive numbers, following physicality arguments, and do not place constraints upon the magnitude of these parameters. The genetic algorithm is halted once the 1000^{th} generation is reached or the average relative change in the best fit determined across successive generations differs by less than 1×10^{-6}. We show the results of this fitting procedure in Figure 2a.

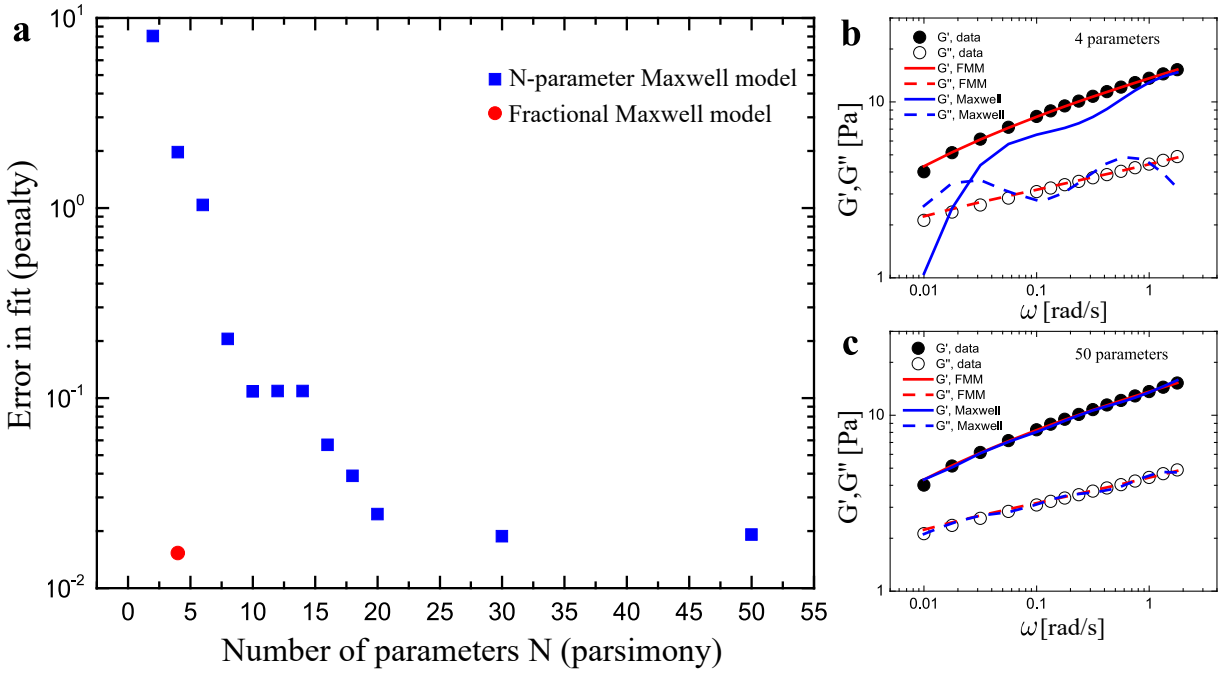

Figure 2: Comparison of the goodness of fit for M-mode Maxwell models against the FMM, as fitted to experimental SAOS data for $c = 1.2\,\text{wt}\,\%$ TUC. In (a), the error (penalty function) is plotted as a function of the number of model parameters N (parsimony) for both models. In (b) and (c), the predictions of the 4 parameter FMM (red lines) and the experimental data (circles) are plotted, along with the model predictions for an M = 2 mode (N = 4 parameter) Maxwell model (b) and an M = 25 mode (N = 50 parameter) Maxwell model (c) (blue lines).

The results in Figure 2 demonstrate the superiority of the FMM over all M-mode Maxwell models tested. Further, for the same number of parameters, the FMM performs almost two orders of magnitude better (as measured by the error in fit) than the M = 2-mode (N = 4-parameter) generalized Maxwell model. These data also indicate that the cost function of the M-mode Maxwell model converges nearly quadratically to a limiting plateau error value (at around 20 parameters or 10 modes). Note that even with 50 parameters the Maxwell model exhibits a greater error than the FMM. We communicate the effect of these errors in Figures 2b and 2c, showing the performance of the FMM and 2-mode Maxwell model (both having four parameters) in Figure 2b, and the FMM with a 25-mode Maxwell model (both having

similar values of the penalty function) in Figure 2c, along with the data to which each model is fitted.

For some of the food solutions we consider in this study, large degrees of shear thinning result in the solvent viscosity playing an important role in the non-linear steady state flow response, particularly at high shear rates. In order to account for this, we introduce a purely viscous element (a dashpot) in parallel with the FMM mechanical elements, resulting in the fractional Jeffreys model (FJM), shown schematically in Figure 1b. The effect of this modification is to guarantee a plateau in the viscosity at high shear rates, η_s, and also results in a linear increase in the loss modulus ($G''(\omega)$) measured in Small Amplitude Oscillatory Shear (SAOS) flow at high frequencies. Analysis of the frequency response using Fourier transforms results in the addition of a purely imaginary term in the complex modulus that is linearly proportional to the oscillation frequency:

$$G^*_{FJM}(\omega) = \frac{\mathbb{V}(i\omega)^\alpha \mathbb{G}(i\omega)^\beta}{\mathbb{G}(i\omega)^\alpha + \mathbb{V}(i\omega)^\beta} + i\eta_s\omega. \tag{6}$$

In order to select the best model (FMM or FJM) for each food solution, both models were fit to the SAOS data using the Matlab function *fminsearch* with the criterion of minimizing the error defined in Equation (5). Subsequently, the model with the lower fitting error ϵ_N was selected as the optimal choice for the given food solution, where

$$\epsilon_N = \frac{1}{2n_{\text{data}}} \sum_{i=1}^{n_{\text{data}}} \left(\frac{|G'_i - G'_{i,\text{fit}}|}{G'_i} \right) + \left(\frac{|G''_i - G''_{i,\text{fit}}|}{G''_i} \right) \times 100\% \tag{7}$$

is a modified version of Equation (5) which estimates the average percent error of the model at each data point. The two exceptions were the okra and chia solutions, for which the low values of the viscoelastic moduli limited the range of frequencies over which $G'(\omega), G''(\omega)$ could be measured. In these cases, the FJM was used (despite it showing a slightly higher ϵ_N) in order to more faithfully reproduce the shear viscosity data. Further discussion of this is provided in Section 4.2.

In the next section, we use these fractional constitutive models to fit both the linear and non-linear experimental rheological data for the TUC solutions at various concentrations, and demonstrate how the values of the quasiproperties resulting from the model fits can serve as indicators of food texture.

3 Fractional rheological modeling of aqueous solutions of Resource ® Thicken Up Clear

3.1 Linear rheology of TUC

We begin by measuring the rheological response of solutions of various concentrations of TUC under the linear deformation of Small Amplitude Oscillatory Shear (SAOS). This particular fluid was selected as a 'benchmark' as a result of its shelf-stability, well controlled and constant composition, and reproducible rheological properties. Strain sweep experiments (not shown in this paper) indicate that the linear viscoelastic regime for TUC solutions extends to $\gamma \lesssim 5\,\%$, with some small amount of variation between the various concentrations. As such, each SAOS measurement was performed at a strain amplitude within this calculated range, varying between $1\,\% \lesssim \gamma \lesssim 3\,\%$ for all TUC solutions tested. The results of these measurements are shown in Figures 3a and 3b.

Using the principle of Time-Concentration-Superposition [33, 34, 35], the data from Figures 3a and 3b are collapsed against the $c = 1.2\,\mathrm{wt}\,\%$ preparation of TUC. For each of the other TUC concentrations, an appropriate shift factor a_c is determined which reduces the frequency of the SAOS data $\omega_r = a_c\omega$, as well as a vertical shift factor b_c which is taken to be the same for both G' and G'' [35]. The rheological master curves resulting from this superposition are shown in Figure 3c, where it is clear that the linear viscoelastic response of all concentrations of TUC can be neatly collapsed to single curves for $G'(\omega_r)$ and $G''(\omega_r)$ respectively. In Figure 3d, we plot these shift factors as a function of TUC concentration. As expected, the vertical shift factor b_c is a nearly monotonically decreasing function of concentration. The frequency shift factor a_c initially exhibits a strong dependence on the solution concentration, but appears to saturate (or, possibly, to shift outside of the experimental range) at high concentrations ($c \gtrsim 2\,\mathrm{wt}\,\%$) as the complex modulus data becomes increasingly power law-like. This change in the shape of the G'' curves between the terminal and high frequency regions has been reported previously in the literature for polystyrene solutions above the entanglement concentration [36], suggesting that $c_e \approx 2\,\mathrm{wt}\,\%$ for the TUC solutions. This value is in reasonable agreement with the reported value of $c_e \approx 0.5\,\mathrm{wt}\,\%$ for pure xanthan gum solutions measured by Choppe et al. [34], given that xanthan gum constitutes only approximately 1/3 of the contents by weight of TUC [37].

In Table 1, the best fitting fractional constitutive model (fractional Maxwell, FMM, or fractional Jeffreys,

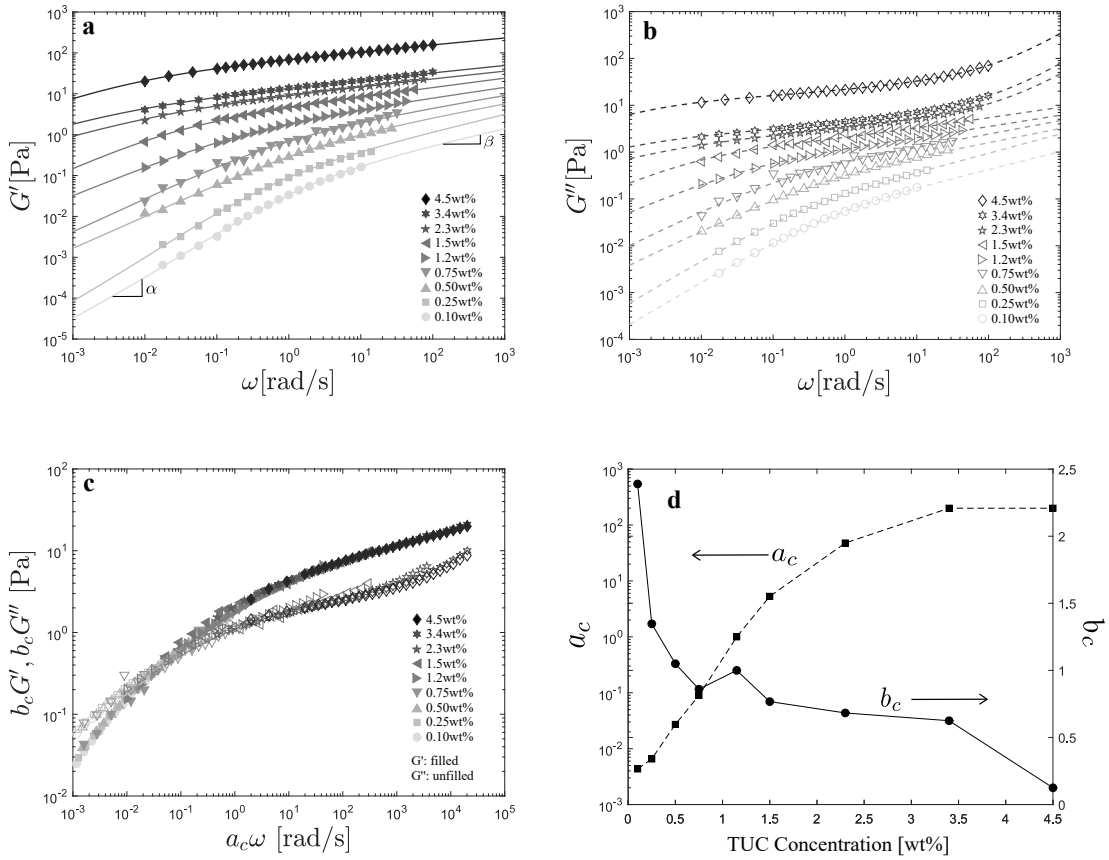

Figure 3: (a) Storage modulus $G'(\omega)$ and (b) loss modulus $G''(\omega)$ for the TUC solutions. The symbols denote the experimentally obtained data and the solid and dashed lines denote the model fits, with individual parameter values specified for each concentration in Table 1. The data from Figures (a) and (b) are shifted to form a master curve using the $c = 1.2\,\mathrm{wt}\,\%$ preparation of TUC as a reference. The frequency is reduced using a shift factor a_c and the moduli $G'(\omega)$ and $G''(\omega)$ are reduced using a common shift factor b_c. The master curves are shown in (c), and the shift factors are plotted as a function of TUC concentration in (d).

FJM), the values of all model parameters, and the value of the fitting error ϵ_N are presented for each TUC concentration tested.

Concentration [wt %]	$\mathbb{V}$ [Pa s$^\alpha$]	α	$\mathbb{G}$ [Pa s$^\beta$]	β	η_s [Pa s]	τ_c [s]	f_{50}	ϵ_N [%]	Model
0.10	0.12	0.92	0.12	0.39	-	9.1×10^{-2}	1.0	2.6	FMM
0.25	0.38	0.93	0.23	0.42	-	1.4×10^{-1}	0.95	3.0	FMM
0.50	0.82	0.76	0.78	0.31	-	5.7×10^{-1}	0.88	2.0	FMM
0.75	2.4	0.77	1.3	0.30	-	1.9×10^{0}	0.78	7.5	FMM
1.2	8.2	0.69	2.8	0.25	-	2.1×10^{1}	0.77	0.83	FMM
1.5	48	0.73	5.4	0.23	-	1.1×10^{2}	0.48	3.4	FMM
2.3	95	0.57	10	0.19	3.6×10^{-2}	$1.5\times10^{4*}$	0.41	1.0	FJM
3.4	260	0.60	15	0.18	6.4×10^{-2}	$1.2\times10^{4*}$	0.42	1.1	FJM
4.5	1100	0.62	75	0.17	2.8×10^{-1}	$3.3\times10^{3*}$	0.41	0.43	FJM

Table 1: FMM and FJM model parameters for the TUC solutions of various concentration. For each solution, the best fitting model (FMM or FJM) is indicated, along with the quasiproperties $\mathbb{V}$ and $\mathbb{G}$, fractional exponents α and β, and solvent viscosity η_s (when appropriate) obtained from the model fits to the experimental data (Equations (1) and (6)). In addition, the characteristic relaxation times τ_c (Equation (4)) and fitting errors (ϵ_N) for the selected models are shown. Finally, the difference between the Cox-Merz prediction and the measured shear viscosity at $\dot{\gamma} = 50\,\mathrm{s}^{-1}$ is denoted by the parameter f_{50} (see [7] and Section 3.2).

It is worth noting, however, that at high TUC concentrations ($c \gtrsim 2\,\mathrm{wt}\,\%$), the crossover frequency $\omega_c = 1/\tau_c$ is below the minimum frequency tested ($\omega_{\min} = 10^{-2}\,\mathrm{rad/s}$). As a result, for these concentrations, τ_c is obtained by extrapolation and is thus less accurately determined. These points are indicated by an asterisk in Table 1.

From Table 1, we observe that for concentrations $c \lesssim 2$wt%, the TUC solutions are better modeled by the FMM than the FJM model. As the moduli of the solutions increase, higher test frequencies can be attained experimentally before the raw phase angle in the linear viscoelastic measurement exceeds 175°. At these high frequencies, the role of the solvent viscosity begins to play an increasingly important role in the SAOS response, and the FJM model (see Figure 2b), with its additional term accounting for the solvent viscosity, is better able to describe the material response. We anticipate that if the SAOS response for the more dilute solutions at similarly high frequencies were able to be obtained, this same contribution from the solvent viscosity would be observed. From the small values of the fitting error ($\epsilon_N \lesssim 10\,\%$) in Table 1 and the fits shown in Figure 3 (solid (G') and dashed (G'') lines, respectively), it

is evident that both models can provide excellent descriptions of the linear viscoelasticity of these xanthan gum-based solutions over a wide range of frequencies ($10^{-2} \leq \omega \leq 10^{2}$ rad/s) with a small number of model parameters.

3.2 Non-linear rheology of TUC

Following the assessment of the linear rheological response of the TUC solutions using SAOS, steady shear flow measurements were performed to determine the nonlinear viscometric response. In Figure 4, the results of these measurements are shown using filled symbols.

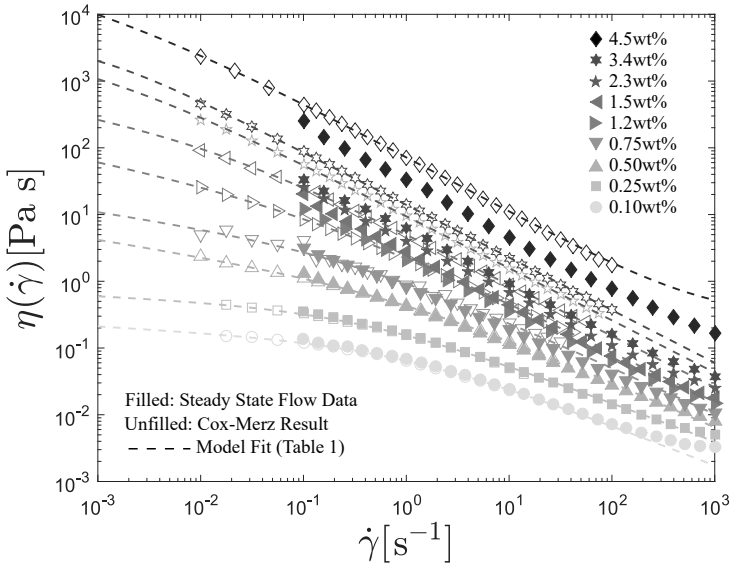

Figure 4: Steady state flow data for the TUC solutions. The filled symbols denote the data obtained experimentally during a steady state flow experiment, the unfilled symbols denote the calculated Cox-Merz result using the SAOS data presented in Figure 3, while the lines denote the fractional model predictions, specified for each concentration in Table 1.

To describe this nonlinear shear rheology data using our fractional models, we use the empiral Cox-Merz rule which relates the complex viscosity to the shear viscosity through the expression [8, 38]

$$\eta(\dot{\gamma})|_{\dot{\gamma}=\omega} \approx |\eta^*(\omega)|. \tag{8}$$

The hollow symbols plotted in Figure 4 show the magnitude of the complex viscosity [8], calculated from the SAOS data for each fluid using the definition

$$|\eta^*(\omega)| = \frac{\sqrt{G'(\omega)^2 + G''(\omega)^2}}{\omega}. \tag{9}$$

Finally, the dashed lines denote the predicted shear viscosity obtained by applying the Cox Merz rule to the complex viscosity calculated from the FMM and FJM expressions for G' and G'' given in Equations (2), (3), and (6). This results in the following expressions:

$$\eta_{\mathrm{FMM}}(\dot{\gamma}) = \frac{\mathbb{V}\mathbb{G}\dot{\gamma}^{\alpha+\beta-1}}{\sqrt{(\mathbb{V}\dot{\gamma}^{\alpha})^2 + (\mathbb{G}\dot{\gamma}^{\beta})^2 + 2\mathbb{V}\dot{\gamma}^{\alpha+\beta}\mathbb{G}\cos(\pi(\alpha-\beta)/2)}} \tag{10}$$

and

$$\eta_{\mathrm{FJM}}(\dot{\gamma}) = \frac{\mathbb{V}\mathbb{G}\dot{\gamma}^{\alpha+\beta-1}}{\sqrt{(\mathbb{V}\dot{\gamma}^{\alpha})^2 + (\mathbb{G}\dot{\gamma}^{\beta})^2 + 2\mathbb{V}\dot{\gamma}^{\alpha+\beta}\mathbb{G}\cos(\pi(\alpha-\beta)/2)}} + \eta_s. \tag{11}$$

From Figure 4, it is clear that for the same range of less concentrated TUC solutions for which the FMM model was better suited than the FJM model ($c \lesssim 2\,\mathrm{wt}\,\%$), the magnitude of the complex viscosity is an excellent approximation of the steady state flow viscosity. Furthermore, for $\alpha \neq 1$, there is no predicted low shear rate plateau viscosity: asymptotic analysis of Equations (10) and (11) shows that the viscosity instead diverges as $\eta(\dot{\gamma}) \sim \dot{\gamma}^{\alpha-1}$ for $\dot{\gamma}\tau_c \ll 1$ although the shear stress still vanishes (as expected at low shear rates) as $\tau_{yx} = \eta(\dot{\gamma})\dot{\gamma} \sim \dot{\gamma}^{\alpha}$. This divergence in shear viscosity with bounded shear stress predicted by the fractional constitutive models is in agreement with what is observed experimentally in many complex biopolymer fluids including saliva and food solutions [7, 39, 40]. Consistent with previous findings for biopolymer solutions, however, as the TUC fluids enter the fully entangled regime ($c > c_e$), the steady shear viscosity predicted using the Cox-Merz rule (Equations (10) and (11)) begins to systematically overestimate the corresponding experimental measurement [7, 38, 40]. Jaishankar and McKinley show that this is because of chain alignment and disentanglement in strong shearing flows which gives rise to a strain-dependent damping function [7]. To quantify this discrepancy, we follow [7] and calculate an offset factor $f_{\dot{\gamma}} = \eta(\dot{\gamma})/|\eta^*(\omega)|$ which indicates the magnitude of the discrepancy. We evaluate this factor at the shear rate widely deemed relevant for oral evaluation of liquid texture, $\dot{\gamma} = 50\,\mathrm{s}^{-1}$ [20],

$$f_{50} \equiv \left.\frac{\eta(\dot{\gamma})}{|\eta^*(\omega)|}\right|_{\omega=\dot{\gamma}=50\mathrm{s}^{-1}} \tag{12}$$

which we also include in Table 1. For the lowest TUC concentration ($c = 0.1\,\mathrm{wt}\,\%$), $f_{50} = 1.01$, which is

reflected in the excellent agreement between the complex and steady state shear viscosities observed in Figure 4. As the TUC concentration is increased, f_{50} begins to decrease, and reaches a plateau value of $f_{50} \approx 0.41$ for the most concentrated solutions, comparable to the value computed analytically by Jaishankar and McKinley [7] using a fractional KBKZ model which incorporates a strain dependent damping function. Nevertheless, we see that from a single rheological test protocol (a frequency sweep in SAOS), the FMM and FJM models provide very good estimates of the steady shear viscosity of TUC solutions over a wide range of shear rates from application of the Cox-Merz rule, with a single correction factor arising from strain-dependent damping in the relaxation modulus at high sample concentrations.

As a final result in this section, we collapse the steady shear viscosity data presented in Figure 4 onto a single master curve, using the concentration-dependent shift factors shown in Figure 3d that were determined from the linear viscoelastic measurements. From Equation (9), it follows that the shifted or reduced value of the steady shear viscosity η_r predicted by the Cox-Merz rule is given by

$$\eta_r(a_c\dot{\gamma}) = \frac{\sqrt{(b_c G'(a_c\dot{\gamma}))^2 + (b_c G''(a_c\dot{\gamma}))^2}}{a_c\omega} = \frac{b_c}{a_c}|\eta^*(a_c\dot{\gamma})|. \tag{13}$$

In Figure (5), we plot the shifted experimental steady state flow data (solid symbols), the shifted values of the dynamic viscosity predicted from the Cox-Merz rule (Equation (9), unfilled symbols), and the shifted predictions of the FMM/FJM models (dashed lines) evaluated using Equation (13) and the model parameters in Table 1. For the sake of clarity and preserving readability, we only show alternate values of the nine TUC concentrations for which steady shear viscosity was collected.

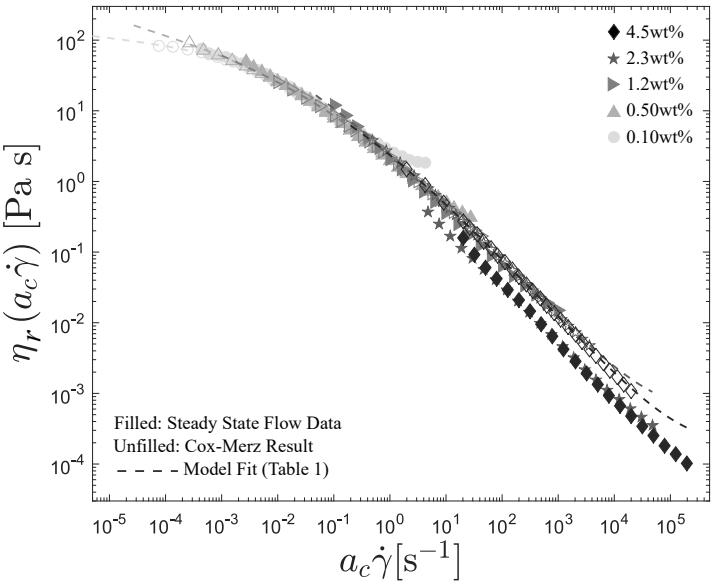

Figure 5: Master curve for steady state flow data of TUC solutions. Only alternate concentrations are shown for clarity. The shift factors a_c and b_c are those determined previously for the G', G'' master curve. The filled symbols denote the data obtained experimentally during a steady state flow experiment, the unfilled symbols denote the calculated Cox-Merz result using the linear viscoelastic data presented in Figure 3, and the lines denote the fractional model predictions using Equation (13) and the model parameters specified for each concentration in Table 1.

As with the linear viscoelastic measurements, the steady shear viscosity data for the TUC solutions collapses quite nicely onto a single master curve. It can be seen, however, that above $a_c\dot{\gamma} \approx 1\,\mathrm{s}^{-1}$ the curves appear to separate onto two distinct branches depending on whether their TUC concentration is greater than or less than the estimated entanglement concentration of $c_e \approx 2\,\mathrm{wt}\,\%$. In this case, for the entangled TUC solutions, the steady shear viscosities calculated using the Cox-Merz rule once again slightly over-predict the steady shear flow measurements [7, 40], and in fact collapse well onto the master curve defined by the lower viscosity (unentangled) solutions.

Having demonstrated how fractional constitutive models can accurately and parsimoniously describe both linear viscoelastic and steady shear rheology data, in the next section, we apply this same framework towards modeling the rheological response of other selected plant extracts whose constituent carbohydrate biopolymers have been previously reported to impart significant viscoelasticity, and to human whole saliva, which is of keen interest in the study of mouth-feel and food textural perception [24].

4 Rheology of food biopolymer solutions and saliva

In this section we use the fractional constitutive models discussed previously to model the rheological response of food biopolymer solutions including two galactomannan heteropolysaccharide solutions: 0.4 wt % tara gum procured from TIC Gums (White Marsh, MD) (3 : 1 ratio of mannose : galactose along its backbone [41]) and 0.5 wt % guar gum procured from Sigma Aldrich (St Louis, MO) (2 : 1 ratio of mannose : galactose along its backbone), as well as extracts from chia seeds, flax seeds, okra, and human whole saliva.

The principal polysaccharide of flax seed (75 % by mass), has a molecular weight of MW $\approx$ 1.2 MDa, and is a neutral arabinoxylan (0.24 : 1 ratio of arabinose : xylose), with sidechains consisting of varying galactose and fucose residues [42]. The principal polysaccharide of chia seed has a molecular weight of MW $\approx 0.8 - 2$ MDa and consists of a mixture of xylose and mannose (17 %), glucose (2 %), galacturonic acid (5 %), and arabinose (2 %) [39]. Flax and chia seed extracts were prepared by combining seeds procured from a local grocery store with deionized water at a mass ratio of 1 : 25 for the flax seeds, following Ziolkovska [42], and 1 : 40 for the chia seeds, following Capitani et al. [39]. Both mixtures were then stirred at 300 rpm on a hot plate at 80 °C for 30 minutes. There was little difficulty in separating the flax seeds from the supernatant, which was generally clear of particulates. In contrast, the chia seed solution required straining through a conventional metal kitchen strainer, with scraping used in order to encourage passage of liquids through the mesh, and then filtering using 100 µm filter paper in order to remove large particulate matter. Thermogravimetric analysis using a Perkin Elmer Pyris 1 Thermogravimetric Analyzer (TGA) revealed that the weight percent of solid particulates in the flax seed solutions was approximately 0.4 wt %, but it was not possible to obtain a similar estimate for the chia seed solutions due to the absence of an obvious plateau in the sample weight following evaporation of the water.

The principal polysaccharide found in okra plants has a molecular weight of MW $\approx$ 1.4 MDa, and consists primarily of galactose, rhamnose, and galacturonic acid [43]. Solutions were prepared using fresh okra plants obtained from a local grocery store. Pods were sliced in half lengthwise following removal of the ends, and the seeds and pith were removed as well. The halves were then cut into approximately 2 cm pieces along their cross-section, and combined with deionized water at a mass ratio of 1 : 10 (plant : water). As with the chia and flax seeds, the cut okra mixtures were stirred at 300 rpm on an 80 °C hot

plate for 30 minutes. The supernatant was then separated from the plants and centrifuged at 2000 rpm for 4 minutes to remove large particulate matter. A similar TGA analysis approximated the solid mass content of the okra extract at 0.1 wt %.

Saliva samples used in this work were obtained without stimulation using the procedure outlined in Frenkel and Ribbeck [44]. Donors were instructed to refrain from eating or drinking for one hour prior to collection. Vacuum was drawn in a closed collection vial using an Amersham VacuGene Pump, into which a tube terminating in the donor's mouth was inserted, and saliva was allowed to accumulate. The collected saliva received no further treatment and was stored at room temperature. Rheological experiments were performed within one hour of collection to ameliorate effects associated with enzymatic degradation of the salivary mucins [45].

4.1 Linear rheology of food biopolymer solutions and saliva

We begin by measuring the linear viscoelastic response of the food biopolymer solutions and saliva and show these results in Figure 6.

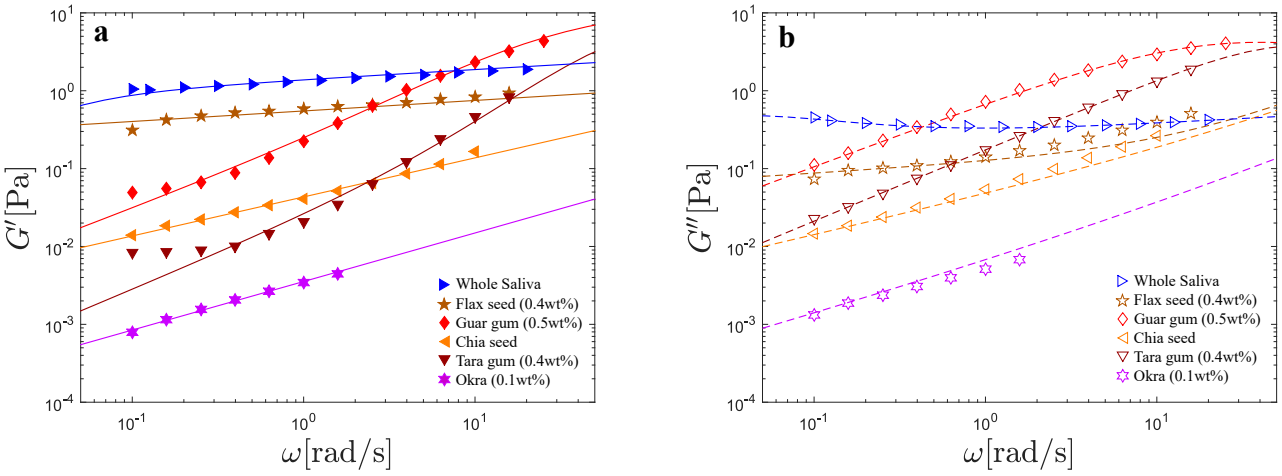

Figure 6: (a) Storage modulus $G'(\omega)$ and (b) loss modulus $G''(\omega)$ for the food biopolymer solutions and saliva. The symbols denote the experimentally obtained data, while the lines denote the model fits, specified for each sample in Table 2. As for the TUC solutions, all SAOS measurements were performed at a strain amplitude within the linear viscoelastic regime of each biopolymer solution as determined by separate strain sweep experiments (results not shown in this paper).

Using the same approach as for the TUC solutions, the FMM or FJM was selected for each biopolymer

solution, and we indicate the best fitting model and corresponding values of the model parameters plus the corresponding fitting errors in Table 2.

Solution	$\mathbb{V}$ [Pa s$^{\alpha}$]	α	$\mathbb{G}$ [Pa s$^{\beta}$]	β	η_s [Pa s]	τ_c [s]	ϵ_N [%]	Model
Chia seed	0.00	-	6.1×10^{-2}	0.50	5.0×10^{-3}	-	8.9	FJM
Flax seed (0.4 wt %)	0.00	-	0.56	0.14	9.0×10^{-3}	-	13	FJM
Okra (0.1 wt %)	0.00	-	6.4×10^{-3}	0.62	1.5×10^{-3}	-	11	FJM
Guar gum (0.5 wt %)	0.74	0.83	7.9	8.2×10^{-2}	-	5.6×10^{-2}	7.4	FMM
Tara gum (0.4 wt %)	0.18	0.92	8.7	0.00	-	1.7×10^{-2}	12	FMM
Whole Saliva	37	1.0	1.4	0.13	-	3.2×10^{1}	4.1	FMM

Table 2: FMM and FJM model parameters for the food solutions and saliva. The material parameters are defined in Equations (2), (3), and (6).

The chia, flax, and okra solutions are relatively weak gels with low viscosities, and are better fit by the FJM with a single dashpot ($\mathbb{V} \to 0$). In constrast, the 0.5 wt % guar gum and 0.4 wt % tara gum as well as whole human saliva are more broadly viscoelastic over a wide range of frequencies and are thus better fit by the FMM. Additional discussion of the model selection for these materials is provided in Section 5. As with the TUC solutions, both models are able to reproduce the experimental data for the biopolymer solutions and saliva well, despite the wide range of differing behaviours and magnitudes of the linear viscoelastic properties observed in the two classes of fluids. However, as a result of inertial limitations to the range over which linear viscoelastic measurements could be performed for the low viscosity food solutions, the high shear rate plateau viscosities measured during steady simple shearing flow for the food solutions that are better fit by the FJM were often not observable in the SAOS response. As such, improving the model fit to the shear viscosity data comes at the cost of poorer agreement with the SAOS data, which explains in part the somewhat higher fitting error ($\epsilon_N \lesssim 15\,\%$) for these solutions. In contrast, for the more viscoelastic TUC solutions, the effects of the background viscosity could be accurately measured for the most concentrated solutions, and the viscoelastic moduli could be accurately measured up to high frequencies in the absence of inertial effects. Consequently, this tradeoff did not exist and the fitting error remained small.

4.2 Non-linear rheology of food biopolymer solutions and saliva

In Figure 7, the steady shear viscosity as a function of shear rate is plotted for the food biopolymer solutions and saliva, with the data divided into two separate plots for clarity. The Cox-Merz rule does a good job of predicting the shear viscosity for the food biopolymer solutions, but it is interesting to note that a significant discrepancy is encountered for whole saliva, as was observed in much more highly concentrated polymer solutions, such as the TUC for $c = 3.4\,\mathrm{wt\,\%}$ or $c = 4.5\,\mathrm{wt\,\%}$ (c.f. Figure 4). This suggests that despite its low values of steady shear viscosity, during the linear deformations of small amplitude oscillatory shear flow, the physical crosslinking present in saliva from electrostatic and hydrophobic interactions [46] plays an important role in the weak gel-like response measured in oscillatory shear, but these effects are largely eliminated during the large strain deformations associated with steady shear flows [7].

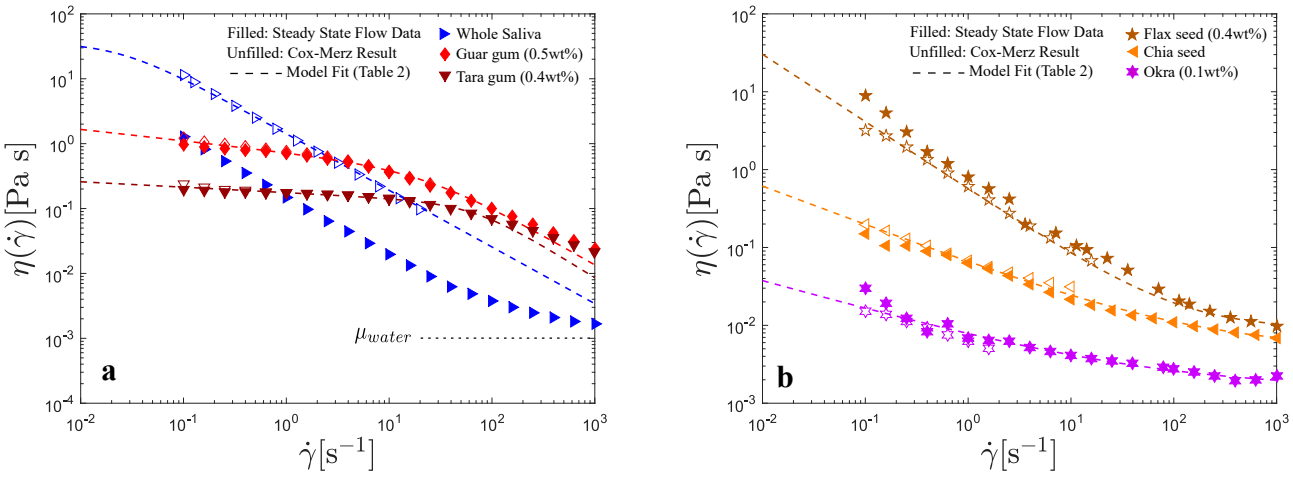

Figure 7: Steady state flow data for the food biopolymer solutions and saliva, divided into two separate plots (a) and (b) for clarity. The filled symbols denote experimental data obtained from steady state flow, and the hollow symbols denote the calculated values using the SAOS data from Figure 6 in conjunction with the Cox-Merz rule. The lines denote the model fits evaluated using Equations (10) and (11), specified for each concentration in Table 2.

5 Rheological interpretation of food consistency and texture using fractional models

The selection of $\dot{\gamma} = 50\,\mathrm{s}^{-1}$ as the shear rate at which viscosity measurements are performed for food texture characterization (including for the 'nectar', 'honey', and 'pudding' standards set by the NDDTF

for starch-based solutions discussed earlier [2]) is generally attributed to the approach devised by F.W. Wood for analyzing his early food sensory panel data [20]. Although Wood acknowledges that 'simple viscosity measurements cannot be used directly to assess the consistency of liquid foods' [20], partially as a result of the different ways that food is handled in the mouth, he nevertheless felt that the range of shearing stresses accessible in the mouth during food consumption must be universal enough for simple characterizations to be meaningful [20]. Consequently, he asked panelists to taste various soups and sauces, and to indicate the Newtonian fluid to which each was closest in consistency [20]. By measuring the steady state flow properties of each of these non-Newtonian soups and sauces, he determined that $\dot{\gamma} = 50\,\mathrm{s}^{-1}$ was the shear rate at which the viscosity of the liquid foods most often matched that of the Newtonian standard to which they were compared, and thus concluded that this must be a relevant characteristic shear rate for food processing in the mouth [20].

In addition to selecting a Newtonian fluid of comparable consistency, many of the panelists in Wood's study reported that they forced the cream or soup to flow by squeezing it between the tongue and the roof of the mouth by raising the tongue suddenly [20]. Interestingly, this selection of a high frequency deformation to comparably assess the various liquid foods is consistent with what is known about the flow behaviour of polymer solutions at different concentrations. As evidenced in Figure 4, as the concentration of a polymer solution is increased, the onset of shear thinning begins at successively lower shear rates [47]. This can be understood by considering the Weissenberg number $\mathrm{Wi} = \dot{\gamma}\tau_c$ for each of these steady state flow curves; a dimensionless parameter quantifying flow nonlinearity that combines the rate of an imposed deformation ($\dot{\gamma}$) and the characteristic relaxation time of the fluid (τ_c). For $\mathrm{Wi} \ll 1$, or relatively weak flows, molecular deformations are able to relax sufficiently quickly to avoid being deformed by the flow, and as a result the fluid behaves essentially in a Newtonian fashion corresponding to the zero-shear-rate plateau. Conversely, once the timescale of rearrangement or relaxation of the constituent polymers exceeds that associated with flow deformation, i.e. $\mathrm{Wi} \gtrsim 1$, the chains are not able to relax sufficiently quickly and thus are forced to align and deform in the flow direction, resulting in the progressive decrease in the fluid viscosity, or shear thinning.

Adam and Delsanti have shown that as the concentration of a polymer solution increases and the chains begin to interact and entangle, the longest viscoelastic relaxation timescale of the fluid scales as $\tau_c \sim (c/c^*)^{3(1-\nu)/(3\nu-1)}$, where c^* is the critical overlap concentration and ν is the excluded volume

exponent [48]. Therefore, for more concentrated polymer solutions with higher crossover times τ_c, shear thinning occurs at smaller values of $\dot{\gamma}$, and from Table 1, it is clear that satisfying $\dot{\gamma} \gtrsim 11\,\mathrm{s}^{-1}$ results in $\mathrm{Wi} \gtrsim 1$ for all of the TUC solutions. Consequently, at the shear rate of $\dot{\gamma} = 50\,\mathrm{s}^{-1}$ proposed by Wood, it is reasonable to expect that all of the TUC solutions are undergoing nonlinear deformation leading to shear thinning in the fluid viscosity, and thus it seems reasonable to compare fluid properties under these flow conditions. If a much smaller shear rate, say $\dot{\gamma} = 1\,\mathrm{s}^{-1}$, were selected, then the measured physical properties of the less concentrated solutions which have not yet begun to shear thin may not be directly comparable with those of the more concentrated ones since they are not experiencing comparable perturbations of the underlying fluid microstructure.

We now proceed to show how fractional constitutive models are able to compactly capture a number of these important ideas. First, we note that from Figures 3a, 3b, and 6, it is clear that while multi-mode models such as the FMM or FJM are required to describe the flow behaviour of these food biopolymer solutions over the entire deformation range probed, at frequencies in the vicinity of $\omega \simeq 50\,\mathrm{rad/s}$ (or $\dot{\gamma} \simeq 50\,\mathrm{s}^{-1}$ from application of the Cox-Merz rule), the storage and loss moduli of all of these solutions can also be well approximated locally by even simpler power law viscoelastic relationships. This observation was formalized by Jaishankar and McKinley [7], who demonstrated using Taylor series expansions that in the absence of non-linear damping, the rate-dependent shear viscosity predicted by the FMM and the Cox-Merz rule takes on the limiting expressions of

$$\lim_{\dot{\gamma} \ll 1/\tau_c} \eta(\dot{\gamma}) \approx \mathbb{V}\dot{\gamma}^{\alpha-1} \tag{14}$$

and

$$\lim_{\dot{\gamma} \gg 1/\tau_c} \eta(\dot{\gamma}) \approx \mathbb{G}\dot{\gamma}^{\beta-1}. \tag{15}$$

Such relationships arise naturally from the response of a single springpot or Scott Blair element, for which the complex moduli can be expressed compactly (following [49]) as

$$G^* = i\omega\eta^* = \mathbb{K}\omega^n(\cos(\pi n/2) + i\sin(\pi n/2)). \tag{16}$$

This result and others for the single Scott Blair element can be obtained from the expressions given

above for the FMM model by setting $\mathbb{V} \to 0$ (plus $\eta_s = 0$ for the FJM). Additionally, for notational uniformity, we have replaced $\mathbb{G}$ with $\mathbb{K}$ and β with n to be consistent with the conventional nomenclature used to describe inelastic power law fluids [8]. The quasiproperty $\mathbb{K}$ is then typically referred to as the 'consistency' of the fluid (with units of $\mathrm{Pa\,s^n}$).

From Equation (16), the steady shear viscosity of a viscoelastic material described by a single springpot can be calculated using the Cox-Merz rule and the magnitude of the complex viscosity as

$$\eta(\dot{\gamma})|_{\dot{\gamma}=\omega} \simeq |\eta^*(\omega)| = \mathbb{K}\omega^{n-1}. \tag{17}$$

Equation (17) implies that iso-viscosity curves for a specified viscosity value (denoted generically by the value $\hat{\eta}$) can be plotted for fixed values of $\dot{\gamma}$ as a function of $\mathbb{K}$ and β. Selecting the shear rate of interest $\dot{\gamma} = 50s^{-1}$ and a viscosity value $\hat{\eta}$, Equation (17) reduces to the constraint

$$\hat{\eta} = \eta(\dot{\gamma} = 50s^{-1}) = \mathbb{K}(50)^{n-1}. \tag{18}$$

Solving for n as a function of $\mathbb{K}$ yields

$$n = [1 + \log\hat{\eta}/\log 50] - \log\mathbb{K}/\log 50. \tag{19}$$

From this equation, it is clear that the slope of these iso-viscosity contours in $\{n, \mathbb{K}\}$ space is set by the desired shear rate of interest, i.e.

$$\left.\frac{dn}{d\log\mathbb{K}}\right|_{\dot{\gamma}=50\mathrm{s}^{-1}} = -\frac{1}{\log 50}$$

and its locus in this space is set by the relative magnitude of $\hat{\eta}$.

Using the limiting expressions for $\eta(\dot{\gamma})$ in Equations (14) and (15) and the relative magnitude of $\dot{\gamma} = 50\,\mathrm{s}^{-1}$ and the crossover frequency $\omega_c = 1/\tau_c$, we select from Tables 1 and 2 the quasiproperty and fractional exponent which characterize this high frequency, predominantly elastic response for the TUC solutions, food extracts, and saliva, and plot these values in Figure 8. We note that for materials described by a single springpot (okra, flax, and chia) for which a crossover frequency does not exist, the same quasiprop-

erty and fractional exponent describe the material response for all frequencies of interest and hence first comparing $\dot{\gamma} = 50\,\mathrm{s}^{-1}$ and ω_c is not necessary. For all other materials except tara gum, $\omega_c < \dot{\gamma} = 50\,\mathrm{s}^{-1}$ and hence we take $\mathbb{K} = \mathbb{G}$ and $n = \beta$, while for tara gum we select $\mathbb{K} = \mathbb{V}$ and $n = \alpha$. In this viscoelastic power law space which is parametrized by the values of $\{n, \mathbb{K}\}$, the lower ordinate axis ($n = 0$) corresponds to the limit of a Hookean solid, and then the abscissa corresponds to the magnitude of the elastic shear modulus $\mathbb{K} = G$. Similarly, the upper ordinate axis $n = 1$ corresponds to the limit of a Newtonian liquid, and then the abscissa corresponds to the viscosity $\mathbb{K} = \eta$. The interior of this parameter space describes in a compact fashion the viscoelastic response of power law fluids. We also plot iso-viscosity contours in Figure 8 (the border lines of the shaded regions) corresponding to the textures named 'nectar', 'honey', and 'pudding' for weakly shear thinning starch solutions specified by the NDDTF.

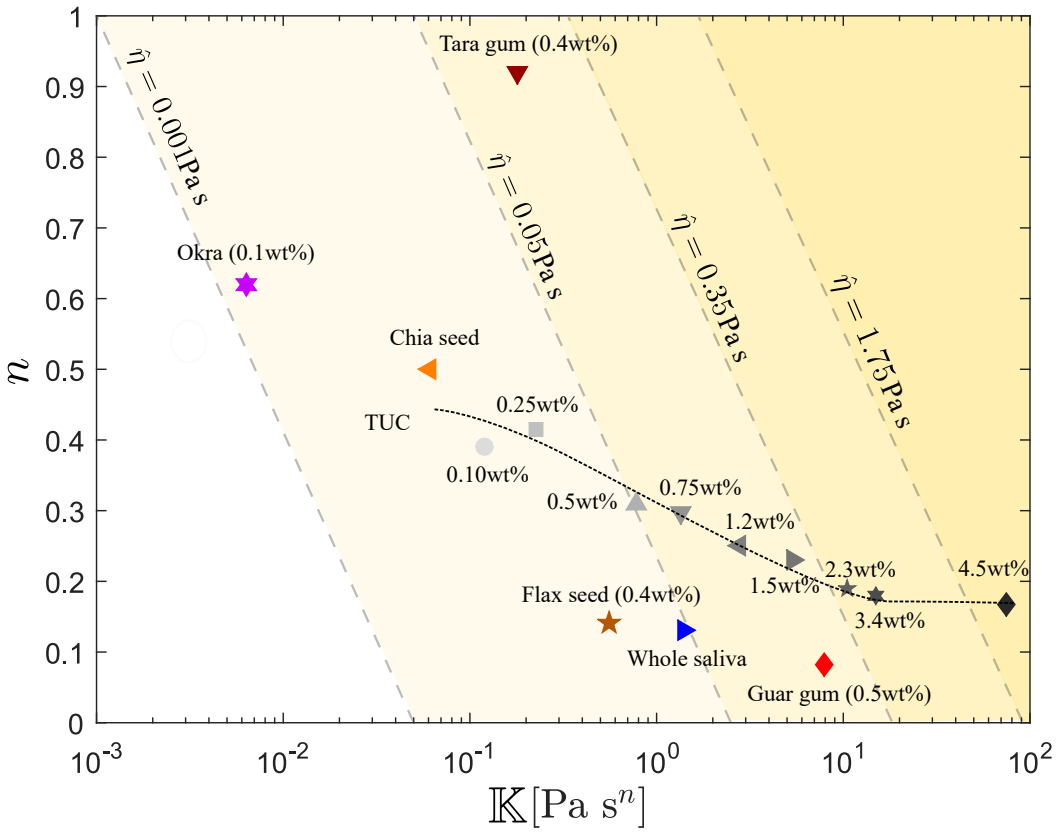

Figure 8: Fractional parameter phase space for food consistency. The markers correspond to the values of the quasiproperty $\mathbb{K}$ and fractional exponent n best describing the shear-thinning in the steady shear viscosity of the TUC solutions, food extracts, and whole saliva at $\dot{\gamma} = 50\,\mathrm{s}^{-1}$. The dashed diagonal lines bordering the shaded regions denote iso-viscosity curves at $\dot{\gamma} = 50\,\mathrm{s}^{-1}$ corresponding to the 'nectar', 'honey', and 'pudding' preparations of starch solutions by the NDDTF. The line connecting the TUC solution markers is a guide for the eye.

As shown in Figure 8, as the concentration of TUC is increased, the quasiproperty $\mathbb{K}$ increases monotonically, affirming its interpretation as an indicator of the viscoelastic modulus of the solution $|G^*| \simeq \mathbb{K}(50)^n$. In conjunction, the fractional exponent n begins at a value of $n \approx 0.40$ for low concentrations, somewhat below the Rouse limit (corresponding to $n = 1/2$ [30]), and then decreases as the TUC concentration is increased before leveling off at a high-concentration plateau of $n \approx 0.18$. A dashed line indicating these trends has been added to the TUC data in Figure 8 as a guide for the eye. It is instructive then to consider the location of the different food extracts and saliva in comparison to this family of TUC solutions. The dependence of the viscoelastic moduli of human whole saliva, flax seed extract, and guar gum on frequency (for frequencies $\omega \approx 50\,\mathrm{rad/s}$) is weaker than those of the most concentrated TUC solutions ($n \approx 0.13$), consistent (from Equation (18)) with higher levels of shear thinning, while the magnitude of their quasiproperty $\mathbb{K}$ is consistent with the TUC solutions of moderate concentrations. The okra and chia seed extracts both exhibit very small values of $\mathbb{K}$, and moderate values of n, near or slightly above the Rouse limit, consistent with classical polymer solutions. Finally, the quasiproperty or consistency $\mathbb{K}$ of the tara gum solution is comparable to those of saliva and the flax seed extract, but its fractional exponent is much higher ($n = 0.92$), corresponding to much lower levels of shear thinning.

Plotting the rheological response of these complex viscoelastic fluids during steady state flow and oscillatory shear in this novel material parameter space allows us to capture both the viscous and elastic characteristics of the fluids, whereas traditional comparison of conventional steady state flow curves or regression to inelastic models such as the Cross or Carreau models fails to discriminate these relevant features. In addition, this representation in $\{n, \mathbb{K}\}$ space makes it strikingly clear that considering the shear viscosity of a solution alone is insufficient to fully characterize its texture. To illustrate this, consider the following exercise. The NDDTF has determined that the lowest shear viscosity at $\dot{\gamma} = 50\,\mathrm{s}^{-1}$ for a food solution to have the texture of a pudding is $\eta(50\,\mathrm{s}^{-1}) = 1.75\,\mathrm{Pa\,s}$. If one were asked to procure a pudding using this criterion, it would be natural to begin with the simplest fluid choice, a Newtonian liquid, and perhaps select maple syrup, which is known to have a viscosity in that range [50]. Since Newtonian fluids are purely viscous, they are characterized using fractional nomenclature as having $n = 1$ and $\mathbb{K} = \mu$. Maple syrup would therefore lie on the line of $\hat{\eta} = 1.75\,\mathrm{Pa\,s}$, at the top of the graph where $n = 1$. Our own experience with eating, however, is likely sufficient to cast doubt on whether maple syrup is the most appropriate choice to mimic a pudding. In more quantitative terms, it appears that a $c \approx 4\,\mathrm{wt\,\%}$ solution of TUC would also satisfy this viscosity criterion, yet its location on the phase space in Figure 8 is at nearly

the opposite end of the ordinate axis, approaching the limit of of $n \to 0$, where a truly 'elasto-plastic' or yield-stress-like response is recovered. More accurate phase boundaries demarcating textures such as 'pudding' must therefore correspond to more complex loci than the straight lines given by Equation (19). It appears as well that since the fractional exponents of all of the TUC solutions and human whole saliva lie below $n = 0.5$, an element of elasticity is essential in the development of dysphagia products, which is consistent with the idea that foods that remain in a cohesive 'bolus' are safer and easier to swallow [51].

6 Conclusions

In this work we have modeled the linear and nonlinear rheological response of a benchmark viscoelastic liquid food, the dysphagia product Resource ® Thicken Up Clear (TUC), as well as various plant extracts and human whole saliva, using fractional rheological models. Using the Matlab genetic algorithm function, we have shown that the FMM does a *better* and more parsimonious job of capturing the rheological response of the TUC solutions (using a representative concentration of $c = 1.2\,\mathrm{wt}\,\%$) than an N-element Maxwell model consisting of up to 50 true physical elements, justifying the use of this more compact representation even at the expense of possible lost physical meaning [27]. We note, however, that for these biopolymer solutions, the breadth of the viscoelastic spectrum is extremely large. The physical meaning of a model containing 10 modes, or 20 parameters (which is the number required for the multi-mode Maxwell model to begin to be comparable to the FMM in terms of goodness of fit to experimental data), becomes increasingly difficult to interpret and unwieldy to use in simulations of viscoelastic flows.

In addition, we have shown that by expressing the viscosity of these liquid foods at the shear rate of $\dot{\gamma} = 50\,\mathrm{s}^{-1}$ (widely deemed relevant for oral evaluation of liquid texture [20]) in terms of the quasiproperty $\mathbb{K}$ and the fractional exponent n arising from these fractional models, far more information about the nonlinear fluid rheology can be gleaned than is usually possible from a traditional steady state flow curve. This extension requires no additional material parameters, but just an application of the Cox-Merz rule. For instance, after ascertaining a characteristic deformation rate for the material of interest, the magnitude of the quasiproperty $\mathbb{K}$ can clearly be interpreted as an indicator of the complex modulus of the solution, while n provides a direct measure of the solution elasticity and the degree of shear thinning. Additionally, by considering the location of the different plant extracts and whole human saliva

in relation to the dysphagia solutions in the phase space formed by $\mathbb{K}$ and n, we can begin to relate these fractional parameters to textural and oral sensory perception terms such as the concepts of a 'pudding' and a 'nectar' in a useful and quantifiable way. Ultimately, we believe that this fractional constitutive framework could be a useful tool for the interpretation of future sensory studies and in the design of liquid food solutions with specifically tailored consistencies or properties.

7 Acknowledgements

The authors would like to thank Nestec Research Center for their support of research in the area of food biopolymer rheology in the HML, and B. Keshavarz and T. Faber for helpful discussions on fractional calculus and its application to food texture. In addition, CEW thanks NSERC (Canada) for a PGS-D award.

8 Footnotes

1. Similarly, Simpson et al. have argued that classical Fickian models are insufficient to describe diffusion processes through food substances, particularly the diffusion of water during dehydration processes, as a result of the morphological changes that these complex fluids undergo on the microscopic level as the water content decreases [52]. They propose that fractional diffusional models, with their non-integer dependence of concentration on both space and time, are more broadly applicable [52].

References

[1] M. Jeltema, J. Beckley, and J. Vahalik. Food texture assessment and preference based on mouth behavior. *Food Quality and Preference*, 52, 2016.

[2] M. M. Ould Eleya and S. Gunasekaran. Rheology of barium sulfate suspensions and pre-thickened beverages used in diagnosis and treatment of dysphagia. *Applied Rheology*, 17(3):1–8, 2007.

[3] M. Nystrom, W. M. Qazi, M. Bulow, O. Ekberg, and M. Stading. Effects of rheological factors on perceived ease of swallowing. *Applied Rheology*, 25(6), 2015.

[4] K. Wendin, S. Ekman, M. Bülow, O. Ekberg, D. Johansson, E. Rothenberg, and M. Stading. Objective and quantitative definitions of modified food textures based on sensory and rheological methodology. *Food and Nutrition Research*, 54:1–11, 2010.

[5] G. W. Scott Blair. Rheology of Foodstuffs, Lecture to the Technical University in Budapest. *Periodica Polytechnica Chemical Engineering*, 16(1):81–84, 1972.

[6] G. W. Scott Blair. The role of psychophysics in rheology. *Journal of Colloid Science*, 2(1):21–32, 1947.

[7] A. Jaishankar and G. H. McKinley. A fractional KBKZ constitutive formulation for describing the nonlinear rheology of multiscale complex fluids. *Journal of Rheology*, 58, 2014.

[8] R. B. Bird, R. C. Armstrong, and O. Hassager. *Dynamics of Polymeric Liquids: Fluid Mechanics (Volume 1)*. Wiley and Sons, 1987.

[9] R. K. Schofield and G. W. Scott Blair. The relationship between viscosity, elasticity and plastic strength of a soft material as illustrated by some mechanical properties of flour dough IV - The separate contributions of gluten and starch. *Proc. R. Soc. Lond. A*, 160, 1937.

[10] J. L. Kokini. Predicting the rheology of food biopolymers using constitutive models. *Carbohydrate Polymers*, 25(4):319–329, 1994.

[11] P. G. Nutting. A new general law of deformation. *Journal of the Franklin Institute*, 191, 1920.

[12] G. W. Scott Blair. Analytical and Integrative Aspects of the Stress-Strain-Time Problem. *Journal of Scientific Instruments*, 21(5):80–84, 1943.

[13] G. W. Scott Blair and J Caffyn. The Classification of the Rheological Properties of Industrial Materials in the light of Power-Law Relations between Stress, Strain and Time. *Journal of Scientific Instruments*, 19(6):88–93, 1942.

[14] G. W. Scott Blair and F. M. V. Coppen. The Subjective Conception of the Firmness of Soft Materials. *The American Journal of Psychology*, 55, 1942.

[15] M. Oroian, S. Amariei, I. Escriche, and G. Gutt. A Viscoelastic Model for Honeys Using the Time-Temperature Superposition Principle (TTSP). *Food and Bioprocess Technology*, 6(9):2251–2260, 2013.

[16] K.-W. Song, H.-Y. Kuk, and G.-S. Chang. Rheology of concentrated xanthan gum solutions: Oscillatory shear flow behaviour. *Korea-Australia Rheology Journal*, 18(2):67–81, 2006.

[17] L. A. Quinchia, C. Valencia, P. Partal, J. M. Franco, E. Brito-de la Fuente, and C. Gallegos. Linear and non-linear viscoelasticity of puddings for nutritional management of dysphagia. *Food Hydrocolloids*, 25(4):586–593, 2011.

[18] T. J. Faber, A. Jaishankar, and G. H. McKinley. Describing the Firmness, Springiness and Rubberiness of Food Gels using Fractional Calculus. Part I: Theoretical Framework. *Food Hydrocolloids*, 62:311–324, 2017.

[19] T. J. Faber, A. Jaishankar, and G. H. McKinley. Describing the Firmness, Springiness and Rubberiness of Food Gels using Fractional Calculus. Part II: Experiments with Cheese. *Food Hydrocolloids*, 62:325–339, 2017.

[20] F. W. Wood. Psychophysical studies on the consistency of liquid foods. Rheology and texture of foodstuffs. In *SCI Monograph No 27*, pages 40–49. London: Society of Chemical Industry, 1968.

[21] M. Atherton, N. Bellis-Smith, J. A. Y. Cichero, and M. Suter. Texture-modified foods and thickened fluids as used for individuals with dysphagia: Australian standardised labels and definitions. *Nutrition and Dietetics*, 64(SUPPL. 2):53–76, 2007.

[22] N. K. Mathur. Less Common Galactomannans and Glucomannans. In *Industrial Galactomannans Polyssaccharides*, pages 145–156. 2012.

[23] N. K. Mathur. Guar Gum. In *Industrial Galactomannans Polyssaccharides*, pages 61–92. 2012.

[24] J. H. H. Bongaerts, D. Rossetti, and J. R. Stokes. The lubricating properties of human whole saliva. *Tribology Letters*, 27(3):277–287, 2007.

[25] C. E. Wagner, A. C. Barbati, J. Engmann, A. S. Burbidge, and G. H. McKinley. Apparent shear thickening at low shear rates in polymer solutions can be an artifact of non-equilibration. *Applied Rheology*, 26(5), 2016.

[26] N. S. Tschoegl. *The phenomenological theory of linear viscoelastic behavior. An introduction.* Springer-Verlag, Berlin, 1989.

[27] J. B. Freund and R. H. Ewoldt. Quantitative rheological model selection: Good fits versus credible models using Bayesian inference. *Journal of Rheology*, 59(3):667–701, 2015.

[28] R. L. Bagley and P. J. Torvik. A Theoretical Basis for the Application of Fractional Calculus to Viscoelasticity. *Journal of Rheology*, 27(1983):201–210, 1983.

[29] R. L. Bagley and P. J. Torvik. On the Fractional Calculus Model of Viscoelastic Behavior. *Journal of Rheology*, 30(1):133–155, 1986.

[30] A. W. Wharmby and R. L. Bagley. Generalization of a theoretical basis for the application of fractional calculus to viscoelasticity. *Journal of Rheology*, 57(5):1429, 2013.

[31] H. Schiessel, R. Metzler, A. Blumen, and T. F. Nonnenmacher. Generalized viscoelastic models: their fractional equations with solutions. *Journal of Physics A: Mathematical and General*, 28, 1995.

[32] A. Jaishankar. *The linear and nonlinear rheology of multiscale complex fluids*. PhD thesis, MIT, 2014.

[33] V. Adibnia and R. J. Hill. Universal aspects of hydrogel gelation kinetics, percolation and viscoelasticity from PA-hydrogel rheology. *Journal of Rheology*, 60:541–548, 2016.

[34] E. Choppe, F. Puaud, T. Nicolai, and L. Benyahia. Rheology of xanthan solutions as a function of temperature, concentration and ionic strength. *Carbohydrate Polymers*, 82(4):1228–1235, 2010.

[35] V. R. Raju, E. V. Menezes, G. Marin, W. W. Graessley, and L. J. Fetters. Concentration and molecular weight dependence of viscoelastic properties in linear and star polymers. *Macromolecules*, 14(6):1668–1676, 1981.

[36] Y. Heo and R. G. Larson. Universal scaling of linear and nonlinear rheological properties of semidilute and concentrated polymer solutions. *Macromolecules*, 41(22):8903–8915, 2008.

[37] Nestle Health Science. Resource Thicken Up Clear. `https://www.thickenupclear.com/`, 2012.

[38] V. Sharma and G. H. McKinley. An intriguing empirical rule for computing the first normal stress difference from steady shear viscosity data for concentrated polymer solutions and melts. *Rheologica Acta*, 51, 2012.

[39] M. I. Capitani, L. J. Corzo-Rios, L. A. Chel-Guerrero, D. A. Betancur-Ancona, S. M. Nolasco, and M. C. Tomas. Rheological properties of aqueous dispersions of chia (Salvia hispanica L.) mucilage. *Journal of Food Engineering*, 149:70–77, 2015.

[40] S. B. Ross-Murphy. Structure–property relationships in food biopolymer gels and solutions. *Journal of Rheology*, 39(1995):1451, 1995.

[41] Y. Wu, W. Ding, L. Jia, and Q. He. The rheological properties of tara gum (Caesalpinia spinosa). *Food Chemistry*, 168:366–371, 2015.

[42] A. Ziolkovska. Laws of flaxseed mucilage extraction. *Food Hydrocolloids*, 26(1):197–204, 2012.

[43] V. Kontogiorgos, I. Margelou, N. Georgiadis, and C. Ritzoulis. Rheological characterization of okra pectins. *Food Hydrocolloids*, 29:356–362, 2012.

[44] E. S. Frenkel and K. Ribbeck. Salivary Mucins Protect Surfaces from Colonization by Cariogenic Bacteria. *Applied and Environmental Microbiology*, 81(1):332–338, 2014.

[45] D. Esser, G. Alvarez-Llamas, M. de Vries, D. Weening, R. J. Vonk, and H. Roelofsen. Sample stability and protein composition of saliva: Implications for its use as a diagnostic fluid. *Biomarker Insights*, 2008(3):25–37, 2008.

[46] R. G. Schipper, E. Silletti, and M. H. Vingerhoeds. Saliva as research material: Biochemical, physicochemical and practical aspects. *Archives of Oral Biology*, 52(12):1114–1135, 2007.

[47] R. K. Gupta. *Polymer and Composite Rheology*. Marcel Dekker, New York, 2nd edition, 2000.

[48] M. Adam and M. Delsanti. Viscosity and longest relaxation time of semi-dilute polymer solutions: II. Theta solvent. *Journal de Physique*, 45(9):1513–1521, 1984.

[49] A. Jaishankar and G. H. McKinley. Power-law rheology in the bulk and at the interface: quasi-properties and fractional constitutive equations. *Proceedings of the Royal Society A: Mathematical, Physical and Engineering Sciences*, (1989):1–21, 2012.

[50] Hydramotion. Hydramotion units of viscosity. `https://hydramotion.com/uploads/view/20160224144736\_Hydramotion\_Viscosity\_Units.pdf`.

[51] A. S. Burbidge and B. J. D. Le Révérend. Biophysics of food perception. *Journal of Physics D: Applied Physics*, 49(11):114001, 2016.

[52] R. Simpson, A. Jaques, H. Nuñez, C. Ramirez, and A. Almonacid. Fractional calculus as a mathematical tool to improve the modeling of mass transfer phenomena in food Processing. *Food Engineering Reviews*, 5(1):45–55, 2013.